Prime editing for functional repair in patient-derived disease models

Imre F. Schene[1,2,3], Indi P. Joore[2,3]*, Rurika Oka[4,5], Michal Mokry[1], Anke H.M. van Vugt[1,3], Ruben van Boxtel[4,5], Hubert P.J. van der Doef[6], Luc J.W. van der Laan[7], Monique M.A. Verstegen[7], Peter M. van Hasselt[2], Edward E.S. Nieuwenhuis[1,8#], Sabine A. Fuchs[1,5,9#]*

1. Division of Pediatric Gastroenterology, Wilhelmina Children's Hospital, University Medical Center Utrecht, Lundlaan 6, 3584 EA Utrecht, the Netherlands.

2. Department of Metabolic Diseases, Wilhelmina Children's Hospital, University Medical Center Utrecht, Lundlaan 6, 3584 EA Utrecht, the Netherlands.

3. Regenerative Medicine Center Utrecht, Uppsalalaan 8, 3584 CT Utrecht, the Netherlands.

4. Princess Maxima Center, 3584 CS Utrecht, the Netherlands

5. Oncode Institute, Princess Maxima Center, 3584 CS Utrecht, the Netherlands

6. Department of Pediatric Gastroenterology, University Medical Center Groningen, Hanzeplein 1, 9713 GZ Groningen, the Netherlands.

7. Department of Surgery, Erasmus MC–University Medical Center Rotterdam, Doctor Molewaterplein 40, 3015 GD Rotterdam, the Netherlands.

8. Department of Sciences, University College Roosevelt, Lange Noordstraat 1, 4331 CB Middelburg, the Netherlands.

9. Corresponding author: s.fuchs@umcutrecht.nl, on behalf of 'United for Metabolic Diseases', The Netherlands.

**These authors contributed equally*

#These authors jointly supervised this work

Abstract

Prime editing is a novel genome editing technology using fusion proteins of Cas9-nickase and reverse transcriptase, that holds promise to correct the vast majority of genetic defects. We develop prime editing for primary adult stem cells grown in organoid culture models. First, we generate precise in-frame deletions in the gene encoding ß-catenin (*CTNNB1*) that result in proliferation independent of Wnt-stimuli, mimicking a mechanism of the development of liver cancer. Moreover, prime editing functionally recovers disease-causing mutations in intestinal organoids from patients with DGAT1-deficiency and liver organoids from a patient with Wilson disease (*ATP7B*). Prime editing is as efficient in 3D grown organoids as in 2D grown cell lines and offers greater precision than Cas9-mediated homology directed repair (HDR). Base editing remains more reliable than prime editing but is restricted to a subgroup of pathogenic mutations. Whole-genome sequencing of four prime-edited clonal organoid lines reveals absence of genome-wide off-target effects underscoring therapeutic potential of this versatile and precise gene editing strategy.

Introduction

The development of gene-editing therapies to treat monogenic diseases has long been an essential goal of CRISPR/Cas9 research. Cas9-mediated homology-directed repair (HDR) can create all desired base substitutions, insertions and deletions (indels). However, HDR relies on introduction of double-stranded DNA breaks, is inefficient and error-prone[1,2]. Base editing, that uses Cas9-nickases fused to DNA-modifying enzymes, is more efficient and accurate than HDR, but can only correct four out of twelve nucleotide substitutions and no small insertions and deletions. Furthermore, base editing requires a suitable protospacer adjacent motif (PAM) and the absence of co-editable nucleotides[3].
Prime editing combines a nicking-Cas9–reverse transcriptase fusion protein (PE2) with a prime editing guide RNA (pegRNA) containing the desired edit. The pegRNA-spacer guides the Cas9-nickase to create a nick in the targeted DNA strand. The pegRNA-extension binds to this nicked strand and instructs the reverse transcriptase to synthesize an edited DNA flap. This edited flap is then integrated by DNA repair mechanisms, which can be enhanced by simultaneous nicking of the non-edited strand (Supplementary Fig. 1)[4].
Prime editing has been applied in human cell lines, plant cells, and mouse embryonic cells but not in human disease models[4,5,6,7]. Adult stem cell-derived organoids exhibit important functional properties of organs, allowing modeling of monogenic diseases[8].

In this work, we develop prime editing in primary patient-derived organoids to show functional correction of disease-causing mutations and generation of representative disease models. We find that prime editing in 3D organoids is as efficient as in 2D cell lines and does not result in detectable genome-wide off-target effects.

Results

Prime editing efficiently creates mutations in organoids

We first optimized prime editing for organoid cells using deletions and single-nucleotide substitutions previously performed in HEK293T cells[4]. The non-edited strand was nicked by a second 'nicking sgRNA' to enhance editing (PE3). Our optimized protocol consisted of co-transfection of prime edit plasmids with a GFP-reporter plasmid allowing selection and subsequent clonal expansion of transfected cells. Prime editing of intestinal and ductal liver organoids resulted in efficient deletion of 5 nucleotides in *HEK3*, with the majority of picked clones containing monoallelic or biallelic deletions (Fig. 1b and Supplementary Fig. 2)[4]. Furthermore, we were able to induce a transversion mutation located 26 nucleotides downstream of the nick in 20% of the clones (Fig. 1c)[4].

Next, we targeted the Wnt-pathway intermediate ß-catenin (*CTNNB1*) in organoids. Activating carcinogenic *CTNNB1* mutations are found in ±40% of hepatocellular carcinoma, resulting in Wnt-signaling independent of exogenous stimuli[9]. We designed PE3 plasmids, containing pegRNA-extensions with primer binding sites (PBSs) and RT-templates of various lengths, that all create in-frame deletions in the ß-TrCP region required for CTNNB1 ubiquitination (Fig. 1d). As wildtype liver organoid expansion depends on Wnt-pathway activation, edited cells could be selected by withdrawing Wnt-agonist R-spondin 1 (Fig. 1e). Sequencing confirmed that all clones grown without R-spondin for two weeks contained heterozygous in-frame deletions in *CTNNB1* (Fig. 1f and Supplementary Fig. 2c). We observed striking differences (up to a factor 50) in editing efficiencies of different pegRNA designs (Fig. 1g). Next, we generated the severe *ABCB11*^{D482G} mutation, a frequent cause of bile salt export pump (BSEP) deficiency[10]. This nucleotide substitution was generated in 20% of the liver organoid clones when silent PAM mutations were introduced (Supplementary Fig. 3). These results demonstrate the utility of prime editing in creating disease models and the importance of testing different pegRNA designs to induce the desired edit.

To examine the efficiency and byproduct formation of prime editing in primary stem cells, we performed high-throughput sequencing of two targeted amplicons (*HEK3* and *CTNNB1*). The desired edit was installed with 30-50% efficiency, while unwanted byproducts at the pegRNA or nickase sgRNA target sites only occurred at a rate of 1-4% in liver- and intestine-derived organoid cells. These rates were similar in two-dimensional HEK293T and Caco-2 cell lines from the same experiment (Fig.

1h). Distinct byproducts were shared between organoid lines and 2D cell cultures, suggesting that the mechanism of byproduct formation is independent of culture type (Supplementary Fig. 4). Together, these results show successful prime editing of primary stem cells with similar efficiency and accuracy as in human cancer cell lines.

Prime editing functionally corrects disease-causing mutations

To investigate prime editing for functional correction of disease-causing mutations, we studied *diacylglycerol-acyltransferase 1* (*DGAT1*) in patient-derived intestinal organoids. *DGAT1* encodes an enzyme catalyzing the conversion of diacylglycerol and fatty acyl-CoA to triacylglycerol. When DGAT1 function is deficient, fatty acids (FAs) cannot be incorporated in lipid droplets and instead cause lipotoxicity and cell death (Fig. 2a). *DGAT1* mutations result in congenital diarrhea and protein-losing enteropathy upon lipid intake[11]. The common biallelic 3-bp deletion (c.629_631delCCT, p.S210del) in exon 7 of *DGAT1* leads to complete absence of the mature protein (Fig. 2b,e)[11]. We designed PE3 plasmids to promote the insertion of the missing three nucleotides. These plasmids were transfected into patient-derived organoid cells and organoids were grown from single transfected cells. PE3 plasmids did not reduce the outgrowth efficiency or proliferation capacity of organoid cells, relative to a GFP-plasmid only control (Supplementary Fig. 5a). Sanger sequencing of clonal organoids revealed repair of the pathogenic deletion (Fig. 2b). To demonstrate DGAT1 function of prime edited cells, we exposed organoids to FAs, which are harmless to healthy control organoids and toxic to DGAT1-deficient organoids (Fig. 2c,d and Supplementary Fig. 5b). All clones surviving functional selection were genetically repaired (Fig. 2c and Supplementary Fig. 6a) and showed normal DGAT1 protein expression (Fig. 2e and Supplementary Fig. 6c). Next, we compared prime editing to HDR in terms of efficiency and accuracy. The ratio of correct editing to unwanted indels was ±30-fold higher for prime editing than for Cas9-initiated HDR (Fig. 2f and Supplementary Fig. 6d). These findings show that prime editing, as opposed to base editing, can repair small deletions with considerably higher precision and efficiency than HDR.

To compare prime editing to base editing, we selected two severe pathogenic G→A mutations suitable for correction by adenine base editors (ABEs): the BSEP-deficiency mutation *ABCB11*^{R1153H} and the alpha-1 antitrypsin deficiency ZZ-genotype (*SERPINA1*^{E342K})[10,12,13]. Without pegRNA design optimization, prime editing was outperformed by base editing in efficiency (Fig. 2g and Supplementary Fig. 7), indicating that the added value of prime editing currently lies in correcting mutations that are uneditable by base editors.

Next, we set out to repair a 1-bp duplication (c.1288dup, p.S430fs) in *ATP7B*, causing Wilson disease. *ATP7B* encodes a copper-transporter (ATP7B), facilitating excretion of excess copper into the bile canaliculus (Fig. 2h). Pathological accumulation of copper in the liver of Wilson disease patients leads to liver cirrhosis requiring lifelong treatment and ultimately liver transplantation[14]. We designed several PE3 conditions to remove the 1-bp duplication in patient-derived liver organoids (Supplementary Fig. 9). Clonal picking of transfected organoid cells confirmed monoallelic repair of the disease-causing mutation by pegRNA#2 (Fig. 2i). We then generated *ATP7B*^{KO} organoids that were more susceptible to copper-induced cell death than *ATP7B*^{WT} organoids (Fig. 2j and Supplementary Fig. 7). To demonstrate functional repair of *ATP7B*^{S430fs} organoids after prime editing, transfected cells were exposed to copper for 4 days (Supplementary Fig. 2). Out of three different pegRNA plasmids, only successful monoallelic repair with pegRNA#2 resulted in rescue of copper excretion (Fig. 2k). These results confirm the ability of prime editing to genetically and functionally correct truncating mutations and underline the importance of testing various pegRNA designs.

Prime editing induces no genome-wide off-target effects

The rate at which genome editors generate undesired mutations across the genome is a major determinant of their therapeutic potential. To date, no genome-wide examination of the fidelity of prime editors has been conducted in human cells. We therefore performed whole-genome sequencing (WGS) analysis on two prime-edited clones and their respective unedited control clones for both the *CTNNB1* 6-bp deletion in liver organoids and the *DGAT1* 3-bp insertion in intestinal organoids. To identify possible variants induced by prime editing, mutational profiles of clones were background-corrected for variants already present in the donor bulk culture (Fig. 3a). At *in silico* predicted off-target sites (204 and 287 for *CTNNB1* and *DGAT1* edits, respectively) no mutations occurred in a range of 200 bp in any of the prime-edited clones (Supplementary Table 4). The total number of new base substitutions or indels was not higher in prime-edited clones compared to controls (Fig. 3b). Specifically, no additional 6-bp deletions or 3-bp insertions appeared (Supplementary Table 4). Furthermore, no clustering of new mutations on a genome-wide scale, known as mutational hotspots, was present in any of the samples (Supplementary Fig. 10b). Ongoing mutational accumulation during cell culture prevents direct attribution of specific mutations to prime editing. We therefore applied mutational signature analysis to search for mutational patterns due to potential aberrant prime editor activity[15,16]. The mutational signatures of prime-edited clones and unedited negative controls (NCs) were highly similar, both resembling the signature that arises during long-term propagation of intestinal organoids *in vitro* (Fig. 3c)[15]. Signatures of negative controls and prime-edited samples could be reconstructed to a comparable degree by the combination of known *in vivo*- and *in vitro*-mutational signatures (cosine similarity

0.92-0.96; Fig. 3d and Supplementary Fig. 10c). This indicates that prime editors do not leave a mutational fingerprint at the genome-wide scale. Safety of prime editing was further confirmed by absence of additional oncogenic mutations in tumor suppressor genes or oncogenes compared to negative controls, apart from the intended 6-bp deletion in CTNNB1 samples (Supplementary Fig. 10d)[17].

Discussion

Versatile, efficient, and safe gene editing in primary cells represents a gamechanger for both *in vitro* modeling of monogenetic diseases and treatment with autologous gene-corrected cells. Here, we provide a protocol for effective prime editing in human adult stem cells. Using this protocol, we demonstrate that prime editing can generate insertions, deletions, and various point mutations and functionally correct disease phenotypes in patient-derived stem cells. We find high editing rates and low byproduct formation in both 3D-cultured adult stem cell organoids and 2D-cultured cancer cell lines. Importantly, prime editing results in higher efficiency and drastically lower indel-formation compared to Cas9-mediated HDR. In the subset of mutations applicable to base editing, prime editors are currently less robust than the latest generation of base editors.

Our data in primary adult stem cells corroborate findings in cancer cell lines and mouse cortical neurons, in which prime editing typically offers greater precision than Cas9-mediated HDR and lower on-target efficiency than base editing, when the target nucleotide is suitably located[4]. Base editing, however, has been subject to various stages of optimization, whereas prime editing is still in its infancy[13,18,19]. The efficiency of prime editing in mammalian and plant cells has been strongly associated with pegRNA design, but optimal PBS and RT-template parameters remain elusive and differ between target sites[4,6,7]. In our hands, pegRNA design also had profound effects on editing efficiency, with PBS lengths of 10-12 nucleotides outperforming longer designs (Fig. 1g and 2k). We expect that pegRNA design as well as the prime editor fusion protein can be further optimized to improve prime editing efficiency in the future.

The WGS analysis provided here constitutes the most comprehensive genome-wide interrogation of prime editor fidelity to date. We did not find any off-target effects at locations resembling the target site. Neither could we identify a mutational signature induced by prime editor enzymes. Despite our small sample size, this absence of genome-wide off-target effects is reassuring for further therapeutic development.

To conclude, this study confirms the potential of prime editing to model and safely repair human monogenic diseases and represents an important step towards future clinical application.

References

1. Chapman, J. R., Taylor, M. R. G. & Boulton, S. J. Playing the End Game: DNA Double-Strand Break Repair Pathway Choice. *Mol. Cell* **47**, 497–510 (2012).
2. Paquet, D. *et al.* Efficient introduction of specific homozygous and heterozygous mutations using CRISPR/Cas9. *Nature* **533**, 125–129 (2016).
3. Rees, H. A. & Liu, D. R. Base editing: precision chemistry on the genome and transcriptome of living cells. *Nat. Rev. Genet.* **19**, 770–788 (2018).
4. Anzalone, A. V. *et al.* Search-and-replace genome editing without double-strand breaks or donor DNA. *Nature* **576**, 149–157 (2019).
5. Xu, R. *et al.* Development of a plant prime editing system for precise editing in the rice genome. *PLANT Commun.* 100043 (2020). doi:10.1016/j.xplc.2020.100043
6. Lin, Q. *et al.* Prime genome editing in rice and wheat. *Nat. Biotechnol.* (2020). doi:10.1038/s41587-020-0455-x
7 Liu, Y. *et al.* Efficient generation of mouse models with the prime editing system. *Cell Discov.* **6**, 27 (2020).
8. Clevers, H. Modeling Development and Disease with Organoids. *Cell* **165**, 1586–1597 (2016).
9. Rebouissou, S. *et al.* Genotype-phenotype correlation of CTNNB1 mutations reveals different ß-catenin activity associated with liver tumor progression. *Hepatology* **64**, 2047–2061 (2016).
10. Strautnieks, S. S. *et al.* Severe Bile Salt Export Pump Deficiency: 82 Different ABCB11 Mutations in 109 Families. *Gastroenterology* **134**, 1203–1214 (2008).
11. van Rijn, J. M. *et al.* Intestinal Failure and Aberrant Lipid Metabolism in Patients With DGAT1 Deficiency. Gastroenterology 155, 130-143.e15 (2018).
12. Huch, M. *et al.* In vitro expansion of single Lgr5 + liver stem cells induced by Wnt-driven regeneration. *Nature* **494**, 247–250 (2013).
13. Huang, T. P. *et al.* Circularly permuted and PAM-modified Cas9 variants broaden the targeting scope of base editors. *Nat. Biotechnol.* **37**, 626–631 (2019).
14. Członkowska, A. *et al.* Wilson disease. *Nat. Rev. Dis. Prim.* **4**, 1–20 (2018).
15. Blokzijl, F. *et al.* Tissue-specific mutation accumulation in human adult stem cells during life. *Nature* **538**, 260–264 (2016).
16. Blokzijl, F. *et al.* MutationalPatterns: comprehensive genome-wide analysis of mutational processes. *Genome Med*. 10, 33, (2018).
17. Forbes, S.A. *et al.* COSMIC: somatic cancer genetics at high-resolution. *Nucleic Acids Res.* **45,** 777–783 (2017).

18. Koblan, L.W. *et al.* Improving cytidine and adenine base editors by expression optimization and ancestral reconstruction. *Nat Biotechnol.* **36**, 843-846 (2018).
19. Miller, S.M., *et al.* Continuous evolution of SpCas9 variants compatible with non-G PAMs. *Nat. Biotechnol.* **38**, 471–481 (2020).

Methods

Study approval and human subjects

The study was approved by the responsible local ethics committees (Institutional Review Board of the University Medical Center Utrecht (STEM: 10-402/K) and Erasmus MC Medical Ethical Committee (MEC-2014-060). Tissue biopsies from liver of a patient with BSEP-deficiency was obtained during a liver transplant procedure in the UMCG, Groningen, and biopsies from duodenum of two patients with DGAT1-deficiency was obtained during diagnostic duodenoscopy in the UMCG, Groningen. Tissue biopsies from livers of patients with Wilson disease and alpha-1 antitrypsin deficiency were obtained during liver transplant procedures in the Erasmus MC, Rotterdam. All biopsies were used after written informed consent.

Organoid culture

Liver and intestinal organoids were cultured and passaged according to previously described protocols[12,20]. In short, liver organoids were plated in matrigel (Corning) and maintained in liver expansion medium (EM), consisting of AdDMEM/F12 (GIBCO) supplemented with 2% B27 without vitamin A (GIBCO), 1.25 mM N-Acetylcysteine (Sigma), 10 mM Nicotinamide (Sigma), 10 nM gastrin (Sigma), 10% RSPO1 conditioned media (homemade), 50 ng/ml EGF (Peprotech), 100 ng/ml FGF10 (Peprotech), 25 ng/ml HGF (Peprotech), 5 mM A83-01 (Tocris), and 10 mM FSK (Tocris). SI organoids were plated in matrigel and maintained in SI EM, consisting of AdDMEM/F12 supplemented with 50% WNT3A-, 20% RSPO1-, and 10% NOG(gin)-conditioned medium (all homemade), 2% B27 with vitamin A (GIBCO), 1.25 mM N-Acetylcysteine, 10 mM Nicotinamide, 50 ng/ml murine-EGF (Peprotech), 500 nM A83-01, and 10 mM SB202190 (Sigma). The medium was changed every 2–4 days and organoids were passaged 1:4 –1:8 every week. After thawing, organoids were passaged at least once before electroporation.

Plasmid cloning

Cloning of pegRNA plasmids was performed according to previously described protocols[4]. In brief, the pU6-pegRNA-GG-Vector (Addgene #132777) was digested overnight with BsaI-HFv2 (NEB) and the 2.2kb fragment was isolated. Oligonucleotide duplexes containing the desired pegRNA spacer, pegRNA extension, and pegRNA scaffold sequences were ordered with the appropriate overhangs and annealed. Annealed pegRNA duplexes were cloned into the pU6-pegRNA-GG-Vector using Golden Gate assembly with BsaI-HFv2 (NEB) and T4 DNA ligase (NEB) in a protocol of 12 cycles of 5 min at 16°C and 5 min at 37°C. For cloning of sgRNAs used for PE3 and ABE-NG, we replaced the BsmBI restriction sites of the sgRNA expression vector BPK1520 by BbsI restriction sites using PCR,

which allowed direct ligation of sgRNA-spacer duplexes[21]. All pegRNA, sgRNA, HDR template, and primers sequences used in this work are listed in Supplementary Tables 1–3 and were synthesized by Integrated DNA Technologies (IDT). pCMV-PE2 (Addgene #132775), pU6-pegRNA-GG-acceptor (Addgene #132777), and NG-ABEmax (Addgene #124163) were gifts from David Liu; BPK1520 (Addgene #65777) was a gift from Keith Joung; pSpCas9(BB)-2A-Puro (PX459, Addgene #62988) was a gift from Feng Zhang.

Electroporation

Before electroporation, organoids were grown under normal conditions in 30 µl Matrigel per well. Two days prior to electroporation, organoids were cultured in medium containing surrogate WNT protein (4 nM). Four wells containing organoids were then dissociated for each condition using TrypLE for 4-5 minutes at 37°C and applying mechanical disruption through pipetting. Cells (1×10^5 to 5×10^5 per transfection) were washed once using Advanced DMEM/F12, resuspended in 80 µl OptiMEM containing Y-27632 (10 µM), and 20 µl DNA mixture was added. For prime editing, the DNA mixture contained 12 µg PE2 plasmid, 5 µg pegRNA plasmid, 2 µg nicking sgRNA plasmid, and 1 µg GFP plasmid. For HDR, the DNA mixture contained 15 µg sgRNA containing-Cas9 plasmid (PX459), 1 µl of 100 µM HDR template, and 1 µg GFP plasmid. For base editing, the DNA mixture contained 15 µg NG-ABEmax plasmid, 4 µg sgRNA plasmid, and 1 µg GFP plasmid. For generation of *ATP7B* knockout organoids, the DNA mixture contained 15 µg sgRNA containing-Cas9 plasmid (PX459) and 1 µg GFP plasmid. The cell-DNA mixture was transferred to an electroporation cuvette and electroporated using a NEPA21 electroporator(NEPA GENE) with 2 × poring pulse (voltage: 175 V, length: 5 ms, interval: 50 ms, polarity: +) and 5 × transfer pulse (voltage: 20 V, length: 50 ms, interval: 50 ms, polarity +/-), as previously described[22]. Cells were removed from the cuvette and transferred into 500 µl OptiMEM containing Y-27632 (10 µM). After 20 minutes, cells were plated in 180 µl matrigel. Upon polymerization of the Matrigel, medium was added containing surrogate WNT protein (4 nM) and Y-27632 (10 µM).

FACS

2-3 days after electroporation using the GFP plasmid, cells were dissociated with TrypLE for 2-3 minutes at 37°C. The cells were washed once using Advanced DMEM/F12 and resuspended in 400 µl FACS buffer (PBS with 2 mM EDTA and 0.5% BSA). FACS was used to filter the GFP+ cell population, selecting specifically for transfected cells (FACS Aria, BD). GFP+ cells were retrieved in medium containing surrogate WNT protein (4 nM) and Y-27632 (10 µM), after which the cells were plated as soon as possible at a cell-concentration of ±300 cells per 30 µl Matrigel. Upon polymerization of the Matrigel, medium was added containing surrogate WNT protein (4 nM) and Y-27632 (10 µM).

Organoid reconstitution and proliferation

The number of organoids in each condition were counted by an automated counting algorithm 7 days after seeding single FACS-sorted cells. Organoid reconstitution was calculated as percentage of [number of organoids at day 7 / number of cells seeded at day 0]. Organoid cell proliferation was measured by quantification of average organoid size at day 7 after seeding single cells. At measurements, organoids were incubated with 1 µM CellTrace Calcein Green AM (Thermo Scientific) for 30 minutes and subsequently imaged by an inverted Olympus IX53 epifluorescence microscope (Tokyo, Japan). Images were analyzed using an automated organoid counting algorithm written in ImageJ and average organoid size was calculated for each condition and normalized to the control condition (GFP only).

Genotyping

Single organoids were picked using a p200 pipette and dissociated using TrypLE for 2-3 minutes at 37°C. Cells were resuspended in 30 µl Matrigel total of which 20 µl was plated. DNA was extracted from the remaining 10 µl Matrigel using the Zymogen Quick-DNA microprep kit according to manufacturer instructions. Q5 high fidelity polymerase was used to amplify the genomic region of interest. The PCR product was purified using the Qiagen PCR clean-up kit according to manufacturer instructions. Resulting product was sent for Sanger sequencing to the Macrogen Europe service EZSeq.

High-throughput DNA sequencing of genomic DNA samples

Genomic sites of interest were amplified from genomic DNA samples and sequenced on an Illumina MiSeq as previously described[4]. Briefly, Illumina forward and reverse adapters (Supplementary Table 3) were used for a first round of PCR (PCR1) to amplify the genomic region of interest. In a second round of PCR (PCR2) each sample was barcoded with unique Truseq DNA Index primers (Illumina). DNA concentration was measured by fluorometric quantification (Qubit, ThermoFisher Scientific) and sequenced on an Illumina MiSeq instrument according to the manufacturer's protocols. Sequencing reads were demultiplexed using MiSeq Reporter (Illumina). Alignment of amplicon sequences to reference sequences was performed by Cas-analyzer in HDR mode, using the unedited sequence as the reference sequence and the desired sequence as HDR donor DNA sequence[23]. Prime editing efficiency was calculated as the percentage of [number of reads with the desired edit/ number of total aligned reads]. For unwanted byproduct analysis at the pegRNA or nickase sgRNA site, a comparison range (R) of 30 bp was used so that 60 bp flanking the predicted nicking site were

considered. Frequency of byproducts was calculated as the percentage of [number of reads with unwanted edits/ number of total aligned reads].

Protein blotting

Organoids were lysed in Laemmli buffer (0.12 M Tris HCl pH 6.8, 4% SDS, 20% glycerol, 0.05 g/l bromophenol blue, 35 mM β-mercaptoethanol). Protein concentration was measured using a BCA assay. For western blotting, equal amounts of protein were separated by SDS-PAGE on a 10% acrylamide gel and transferred to PVDF membranes using a Trans-Blot® Turbo machine (Bio-rad) according to manufacturer's protocol. For dot blotting, protein was directly loaded on PVDF membranes without SDS-PAGE separation. The membrane was blocked with 5% milk protein in TBST (0.3% Tween, 10 mM Tris-HCl pH 8 and 150 mM NaCl in distilled water) and probed with primary antibodies against DGAT1 (ab181180; 1:000; Abcam) or ACTB (sc-47778; 1:5000, Santa Cruz Biotechnology) overnight at 4°C. After incubation with HRP-conjugated secondary antibodies (1:5000, DAKO p0260 and p0217, 1h at RT), bands or dots were imaged on a chemiluminescence detection system (Bio-rad).

Functional assays

To select liver organoids with in-frame mutations in *CTNNB1*, organoids were cultured in normal culture medium without R-spondin 1 for two weeks. To test DGAT1 function in intestinal organoids, 4 mM oleic acid was added to the culture medium for 24h and organoid survival was assessed by visual inspection and survival after passaging. To test ATP7B function in liver organoids, copper(II)chloride ($CuCl_2$) was added to the culture medium for 3-4 days. Cell death was quantified by addition of propidium iodide (PI) (0.1 mg/mL, ThermoFisher) to the culture medium for 15 minutes. Organoids were imaged by an inverted Olympus IX53 epifluorescence microscope. PI signal was quantified using ImageJ and normalized to a positive control condition for cell death (1 mM $CuCl_2$). Based on *ATP7B*^{KO} lines, prolonged organoid survival in 0.25 mM $CuCl_2$ was considered as a characteristic of functional ATP7B.

Whole-genome sequencing and mapping

Genomic DNA was isolated from ±5*10^5 cells using the Zymogen Quick-DNA microprep kit according to manufacturer instructions. Standard Illumina protocols were applied to generate DNA libraries for Illumina sequencing from 20-50ng of genomic DNA. All samples (two genetically corrected clones, one non-corrected control sample, and one 'bulk' samples from the starting culture for both the CTNNB1 6bp-deletion and DGAT1 3bp-insertion) were sequenced (2x150bp) using Illumina NovaSeq to 30x base coverage. Reads were mapped against human reference genome hg19 using Burrows-

Wheeler Aligner v0.5.9[24] with settings 'bwa mem -c 100 -M'. Duplicate sequence reads were marked using Sambamba v0.4.7.32 and realigned per donor using Genome Analysis Toolkit (GATK) IndelRealigner v2.7.2 and quality scores were recalibrated using the GATK BaseRecalibrator v2.7.2. More details on the pipeline can be found on Github[25].

Mutation calling and filtering

Raw variants were multisample-called by using the GATK HaplotypeCaller v3.4-46[26] and GATK- Queue v3.4-46 with default settings and additional option 'EMIT_ALL_CONFIDENT_SITES'. The quality of variant and reference positions was evaluated by using GATK VariantFiltration v3.4-46 with options '-snpFilterName LowQualityDepth -snpFil- terExpression ''QD < 2.0'' -snpFilterName MappingQuality -snpFilterExpression ''MQ < 40.0'' -snpFilterName StrandBias - snpFilterExpression ''FS > 60.0'' -snpFilterName HaplotypeScoreHigh -snpFilterExpression ''HaplotypeScore > 13.0'' -snpFilter- Name MQRankSumLow -snpFilterExpression ''MQRankSum < 12.5'' -snpFilterName ReadPosRankSumLow -snpFilterExpression ''ReadPosRankSum <8.0'' -cluster 3 -window 35'. To obtain high-quality somatic mutation catalogs, we applied post processing filters as described[16]. Briefly, we considered variants at autosomal chromosomes without any evidence from a paired control sample ('bulk' starting culture); passed by VariantFiltration with a GATK phred-scaled quality score R 250; a base coverage of at least 20X in the clonal and paired control sample; no overlap with single nucleotide polymorphisms (SNPs) in the Single Nucleotide Polymorphism Database v137.b3730; and absence of the variant in a panel of unmatched normal human genomes (BED-file available upon request). We additionally filtered base substitutions with a GATK genotype score (GQ) lower than 99 or 10 in the clonal or paired control sample, respectively. For indels, we filtered variants with a GQ score lower than 99 in both the clonal and paired control sample and filtered indels that were present within 100 bp of a called variant in the control sample. In addition, for both SNVs and INDELs, we only considered variants with a mapping quality (MQ) score of 60 and with a variant allele frequency of 0.3 or higher in the clones to exclude *in vitro* accumulated mutations[16]. The scripts used are available on Github[27]. The distribution of variants was visualized using an in house developed R package (MutationalPatterns)[16].

In silico off-target prediction

Potential sgRNA specific off-target events were predicted using the Cas-OFFinder open recourse tool[28]. All potential off-targets up to 4 mismatches were taken into account.

Mutational signature analysis

We extracted mutational signatures and estimated their contribution to the overall mutational profile as described using an in house developed R package (MutationalPatterns)[16]. In this analysis, we included small intestine data (previously analyzed)[15] to explicitly extract *in vivo* and *in vitro* accumulated signatures[16].

Statistics and reproducibility

No pre-specified effect size was calculated, and no statistical method was used to predetermine sample size. The source data for figures can be found in Supplementary Table 5. For comparisons of multiple groups, an ordinary one-way ANOVA with Holm–Sidak correction for multiple comparisons was used and performed in Prism (GraphPad Software). All graphs were plotted using Prism (GraphPad Software). In Fig. 1g and Fig. 2d the negative control and the healthy control, respectively, were excluded from statistical comparisons. Statistical tests were appropriate for comparisons being made; assessment of variation was carried out but not included. Experiments were not randomized. Investigators were not blinded to allocation during experiments but outcome assessment (sequencing and functional assay quantification) were performed blinded. Reproducibility: Fig. 1b representative of 12 and 10 clonal liver and intestinal organoids, respectively, each from two independent transfection experiments. Fig. 1c and Fig. 1f representative of 10 clonal liver organoids, from two and three independent transfection experiments, respectively. Fig. 1g representative of three transfection experiments using the same liver organoid donor. Fig. 1h representative of three biological replicates from one transfection experiment. Fig. 2c representative of 20 clonal organoids from two independent experiments. Fig. 2d representative of three independent transfection experiments in two different donors. Fig. 2e and Supplementary Fig 6c represent a single blotting experiment. Fig. 2f representative of 24 and 32 clonal organoids from two independent experiments. Fig. 2g representative of 10 clonal liver organoids per condition, collected through two independent experiments. Fig. 2j represents a single experiment. Fig. 2k representative of two experiments. Fig. 3 and Supplementary Fig. 10 represent a single experiment with two edited clones and one negative control for each of two prime edits. Supplementary Fig. 3 representative of 30 clonal liver organoids from two independent experiments. Supplementary Fig. 5b are representative images for three independent transfection experiments.

Data and material availability

Source data for the figures are provided as a Source Data file. The WGS samples of Fig. 3 and Supplementary Fig. 10 have been submitted to the European Genome-phenome Archive under study number EGAS00001004611 [https://ega-archive.org/studies/EGAS00001004611]. All other data and material supporting the findings of this study are available from the corresponding author on reasonable request.

Code availability

Cas-Analyzer is publicly available [http://www.rgenome.net/cas-analyzer]. The algorithms used for mapping [https://github.com/UMCUGenetics/IAP], mutational calling [gatk.broadinstitute.org], mutational filtering [https://github.com/ToolsVanBox/SMuRF], and mutational pattern analysis [https://www.bioconductor.org/packages/release/bioc/html/MutationalPatterns.html] of WGS data are all publicly available. Cas-OFFinder was used for in silico prediction of off-target sites of pegRNA and sgRNA spacers and is available at [http://www.rgenome.net/cas-offinder/]. The algorithms to quantify the number and size of organoids, as well as to quantify the signal of propidium iodide, were written in ImageJ and are available from the corresponding author on reasonable request.

References

20. Sato, T. *et al.* Single Lgr5 stem cells build crypt-villus structures in vitro without a mesenchymal niche. *Nature* **459**, 262–265 (2009).
21. Ran, F. A. *et al.* Genome engineering using crispr-cas9 system. *Chromosom. Mutagen. Second Ed.* **8**, 197–217 (2014).
22. Fuji, M. *et al.* Efficient genetic engineering of human intestinal organoids using electroporation. *Nat Protoc* **10**, 1474–1485 (2015).
23. Park, J. *et al.* Cas-Analyzer: an online tool for assessing genome editing results using NGS data. *Bioinformatics* **33**, 286-288 (2017).
24. Li, H., and Durbin, R. Fast and accurate long-read alignment with Burrows-Wheeler transform. *Bioinformatics* **26**, 589–595 (2010).
25. Ernst, R. F. et al. UMCUGenetics/IAP: v2.8.0. (Zenodo, 2020). doi:10.5281/ZENODO.3739255.
26. DePristo, M.A., *et al.* A framework for variation discovery and genotyping using next-generation DNA sequencing data. *Nat. Genet.* **43**, 491–498 (2011).
27. Roosmalen, M. V. & Manders, F. ToolsVanBox/SMuRF: SMuRF release v1.0. (Zenodo, 2020). doi:10.5281/ZENODO.4032643
28. Bae, S. *et al.* Cas-OFFinder: a fast and versatile algorithm that searches for potential off-target sites of Cas9 RNA-guided endonucleases. *Bioinformatics* **30**, 1473–1475 (2014).

Acknowledgements

We thank M. Geurts (Hubrecht Institute, the Netherlands) for providing WNT surrogate and for sharing his experiences with Prime Editing. We thank Henkjan J. Verkade sharing unique patient-derived material. This work was supported by Metakids funding (to S.A.F.) and a Clinical Fellows grant from The Netherlands Organisation for Health Research and Development Health Institute (40-00703-97-13537 to S.A.F.).

Author information

These authors contributed equally: Imre F. Schene and Indi P. Joore.

These senior authors contributed equally: Edward E.S. Nieuwenhuis and Sabine. A. Fuchs.

Affiliations

Division of Pediatric Gastroenterology, Wilhelmina Children's Hospital, University Medical Center Utrecht, Utrecht, the Netherlands

Imre F. Schene, Michal Mokry, Anke H.M. van Vugt, Edward E.S. Nieuwenhuis, Sabine A. Fuchs

Department of Metabolic Diseases, Wilhelmina Children's Hospital, University Medical Center Utrecht, Utrecht, the Netherlands

Imre F. Schene, Indi P. Joore, Peter M. van Hasselt, Sabine A. Fuchs

Regenerative Medicine Center Utrecht, Utrecht, the Netherlands

Imre F. Schene, Indi P. Joore, Anke H.M. van Vugt

Princess Maxima Center, Utrecht, the Netherlands

Rurika Oka, Ruben van Boxtel

Department of Pediatric Gastroenterology, University Medical Center Groningen, Groningen, the Netherlands

Hubert P.J. van der Doef

Department of Surgery, Erasmus MC–University Medical Center, Rotterdam, the Netherlands

Luc J.W. van der Laan, Monique M.A. Verstegen

Department of Sciences, University College Roosevelt, Middelburg, the Netherlands

Edward E.S. Nieuwenhuis

Author Contributions

I.F.S., I.P.J., R.B., E.E.S.N., and S.A.F. designed the project; H.P.J.D., L.J.W.K., and M.M.A.V. helped establishing the biobank of patient-derived stem cell organoids used in this study, I.F.S., I.P.J., and A.J.M.v.V. performed experiments and analysis; R.O. performed analyses; I.F.S., I.P.J., M.M., P.M.v.H., E.E.S.N., and S.A.F. wrote the manuscript.

Corresponding author

Correspondence to Sabine A. Fuchs.

Ethics declarations

Conflict of interest

Authors declare that they have no conflicts of interest.

Supplementary information

Supplementary Figure 1: Overview of the prime editing-principle

Supplementary Figure 2: Representative FACS plot example and different protocols used in this study

Supplementary Figure 3: Generation of *ABCB11*^{D482G} by prime editing (PE3)

Supplementary Figure 4: Analysis of editing byproducts after prime editing in HEK293T cells, Caco-2 cells, and liver and intestinal organoid cells

Supplementary Figure 5: Functional correction of *DGAT1*^{S210del} by prime editing (PE3)

Supplementary Figure 6: Prime editing (PE3) and Cas9-mediated HDR to correct *DGAT1*^{S210del}

Supplementary Figure 7: Correction of *ABCB11*^{R1153H} and *SERPINA1*^{E342K} by base editing

Supplementary Figure 8: Validation of a functional assay for ATP7B function

Supplementary Figure 9: PegRNA designs used for correction of ATP7B^{S410fs}

Supplementary Figure 10: Prime editing induces no genome-wide off-target effects

Supplementary Table 1: Sequences of pegRNAs used in this study

Supplementary Table 2: Sequences of sgRNAs and HDR templates used in this study

Supplementary Table 3: Sequences of PCR and sequencing primers used in this study

Supplementary Data 1: *In silico* predicted off-target sites, SNV, and indel counts for WGS

Source Data: Source data for figures

Figure Legends

Figure 1: Prime editing efficiently creates deletions and point mutations in organoids

a, Schematic overview of the workflow and timeline to generate precise mutations in organoid cells using prime editing (PE3). **b**, pegRNA design, Sanger validation in a clonal organoid with monoallelic edit, and editing efficiency of a 5-bp deletion in *HEK3* in liver and intestinal organoids. **c**, pegRNA design, Sanger validation of monoallelic edit, and editing efficiency for a C→G substitution in *HEK3* in liver organoids. Nicking sgRNA at +90 used in **(b)** and **(c)** not shown. **d**, pegRNA designs for the generation of in-frame deletions in the ß-TrCP region of *CTNNB1*. Nicking sgRNA at +86 (S1) or +93 (S2) not shown. **e**, Brightfield images of liver organoid cells transfected with plasmids from **(d)** after Rspo1 withdrawal for 2 weeks. White scale bars are 500 µm. **f**, Sanger validation of precise 6-bp deletions in all picked clones from *CTNNB1* pegRNA S1E1 that continue growing in -Rspo1 conditions. **g**, Quantification of organoid outgrowth in **(e)**. $p<0.0001$ in a one-way ANOVA with Holm–Sidak correction. **h,** Comparison of editing efficiencies and generation of unwanted byproducts in different cell types by high-throughput sequencing (HTS). Only transfected cells (GFP^+ sorted) were used for HTS. Data are represented as mean values +/- S.D. of three independent experiments **(g)** or biological replicates **(h)**. FA: fatty acids, PBS: primer binding site, RTT: reverse transcriptase template. NC: negative control. Source data are provided as a Source Data file.

Figure 2: Prime editing functionally corrects disease-causing indel mutations in intestinal and liver organoids

a, Schematic overview of the DGAT1 disease mechanism. **b,** Sanger validation of biallelic *DGAT1*^{S210del} mutations in patient-derived intestinal organoids, pegRNA design (nicking sgRNA at position +46 not shown), and Sanger validation of successful biallelic correction by PE3. **c,** Brightfield images of healthy control- and *DGAT1*^{S210del} patient-derived intestinal organoids (±PE3) after exposure to 4 mM OA for 24h and subsequent passaging (split). White scale bars are 500 µm. Quantification of corrected alleles in patient organoids after PE3 and OA selection; all surviving organoids are gene-corrected. **d,** Quantification of *DGAT1*^{S210del} patient organoid survival upon exposure to 4 mM OA, after targeting with different PE3 or PE3b plasmids. Data are represented as mean +/- S.D. of three independent experiments in two different donors. **e,** Western blot of DGAT1 in *DGAT1*^{S210del}, healthy control, and PE3-corrected *DGAT1*^{S210del} organoids. **f,** Quantification of correct edits and unwanted indels by PE3 and Cas9-initiated HDR in *DGAT1*^{S210del} organoids. Note that no functional selection with OA was performed prior to quantification. **g,** Comparison of PE3 and adenine base editing (ABEmax-NG) to correct the *ABCB11*^{R1153H} and *SERPINA1*^{E342K} mutations in liver organoids from patients with BSEP-deficiency and alpha-1-antitrypsin deficiency, respectively. **h,** Schematic overview of the Wilson

disease (ATP7B deficiency) mechanism. **i,** Sanger validation of biallelic *ATP7B*^{S430fs} mutations in patient-derived liver organoids, pegRNA#2 design to target this mutation, and Sanger validation of successful monoallelic correction by PE3. **j,** Cell death in *ATP7B*^{WT} and *ATP7B*^{KO} liver organoids after incubation with Cu^{2+} for 3 days. n = 2 biologically independent samples for both WT and KO groups. **k,** Brightfield images of *ATP7B*^{S430fs}-patient organoid survival upon exposure to 0.25 mM Cu2+ for 3 days, after transfection with different PE3 plasmids. 'at -39' stands for nicking sgRNA at position -39. Note that only prime editing using pegRNA#2 yields functional correction of *ATP7B* (white arrowheads). White scale bars are 500 µm. ER: endoplasmic reticulum, FFA: free fatty acid, Ex: exon, NC: negative control, OA: oleic acid, PE3+m: PE3 with introduction of PAM mutation, HDR: homology directed repair, ABE: adenine base editor, PI: propidium iodide. Source data are provided as a Source Data file.

Figure 3: Prime editing induces no genome-wide off-target effects

a, Schematic overview of the protocol used to identify mutations induced by prime editing (PE3). WGS was performed for one unedited negative control and two prime-edited clonal lines for both DGAT1 (intestinal organoids) and CTNNB1 (liver organoids). **b**, Total number of single nucleotide variants (SNVs) and insertions and deletions (indels) in control (NC) and prime-edited (PE3) clonal organoid lines (n = 2 and n = 4 biologically independent samples, respectively). Error bars represent S.D. **c,** Mutational signature analysis by relative contribution of context-dependent mutation types in an *in vivo* (n = 6) and *in vitro* (n = 6) dataset (Blokzijl et al., 2016) and in control and prime edited clonal organoid lines. **d**, Relative contribution of known *in vivo* and *in vitro* mutational signatures from Blokzijl et al. (2016) in control (NC) and prime-edited (PE3) clonal organoid lines (n = 2 and n = 4 biologically independent samples, respectively). Dotted line at 0.9 indicates highly accurate signature reconstruction. NC: negative control, WGS: whole genome sequencing.

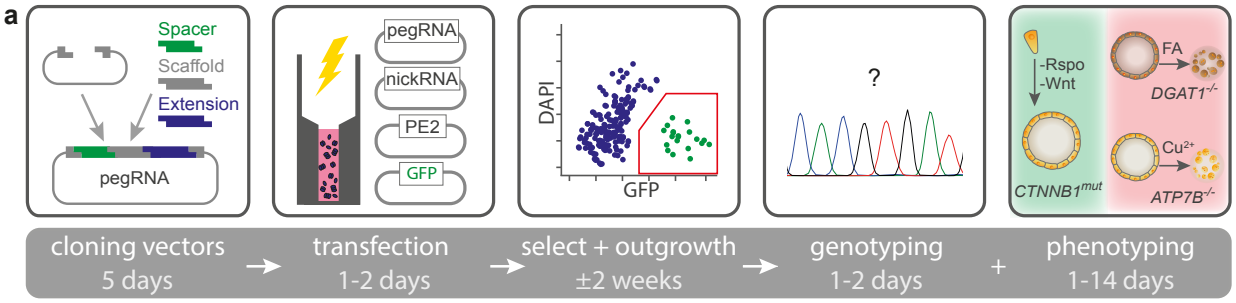
a
Spacer
Scaffold
Extension
pegRNA
pegRNA
nickRNA
PE2
GFP
DAPI
GFP
?
-Rspo
-Wnt
FA
DGAT1-/-
Cu2+
ATP7B-/-
CTNNB1mut
cloning vectors
5 days
transfection
1-2 days
select + outgrowth
±2 weeks
genotyping
1-2 days
+
phenotyping
1-14 days

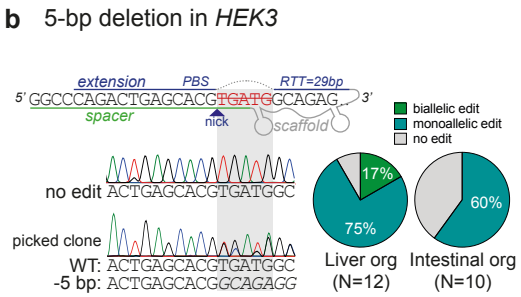
b 5-bp deletion in HEK3
extension
PBS
RTT=29bp
5' GGCCCAGACTGAGCACGTGATGGCAGAG 3'
spacer
nick
scaffold
biallelic edit
monoallelic edit
no edit
no edit ACTGAGCACGTGATGGC
picked clone
WT: ACTGAGCACGTGATGGC
-5 bp: ACTGAGCACGGCAGAGG
17%
75%
60%
Liver org
(N=12)
Intestinal org
(N=10)

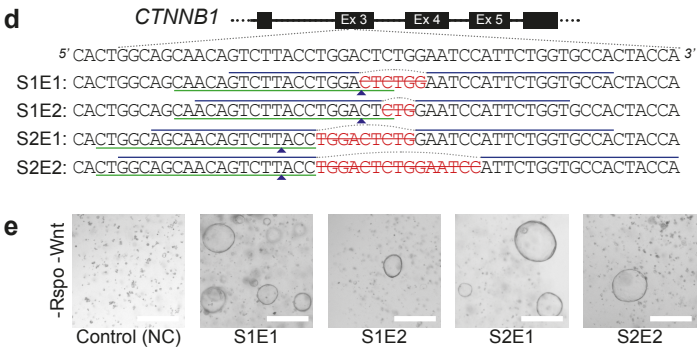
d
CTNNB1
Ex 3
Ex 4
Ex 5
5' CACTGGCAGCAACAGTCTTACCTGGACTCTGGAATCCATTCTGGTGCCACTACCA 3'
S1E1: CACTGGCAGCAACAGTCTTACCTGGACTCTGGAATCCATTCTGGTGCCACTACCA
S2E1: CACTGGCAGCAACAGTCTTACCTGGACTCTGGAATCCATTCTGGTGCCACTACCA
S2E2: CACTGGCAGCAACAGTCTTACCTGGACTCTGGAATCCATTCTGGTGCCACTACCA
e
-Rspo -Wnt
Control (NC)
S1E1
S1E2
S2E1
S2E2

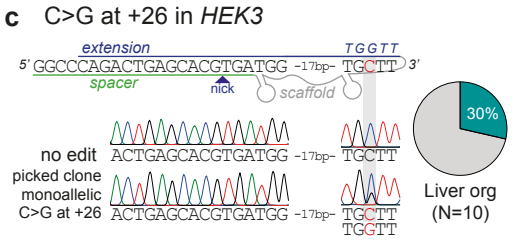
c C>G at +26 in HEK3
extension
TGGTT
5' GGCCCAGACTGAGCACGTGATGG -17bp- TGCTT 3'
spacer
nick
scaffold
no edit ACTGAGCACGTGATGG -17bp- TGCTT
picked clone
monoallelic
C>G at +26 ACTGAGCACGTGATGG -17bp- TGCTT
TGGTT
30%
Liver org
(N=10)

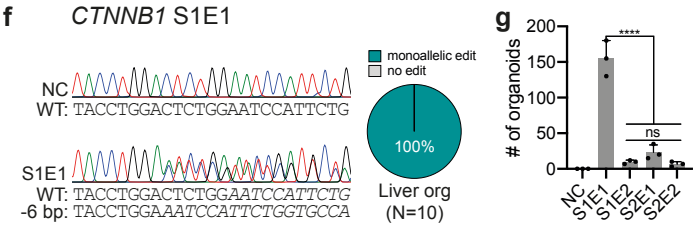
f CTNNB1 S1E1
NC
WT: TACCTGGACTCTGGAATCCATTCTG
S1E1
WT: TACCTGGACTCTGGAATCCATTCTG
-6 bp: TACCTGGAAATCCATTCTGGTGCCA
monoallelic edit
no edit
100%
Liver org
(N=10)
g
# of organoids
200
150
100
50
0
****
ns
NC
S1E1
S1E2
S2E1
S2E2

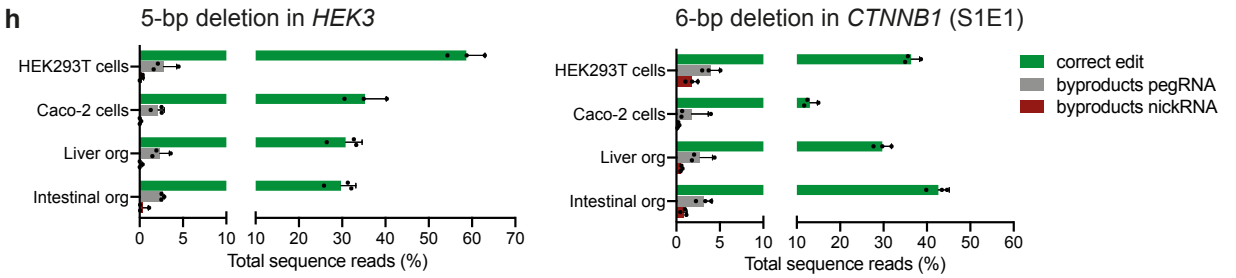
h 5-bp deletion in HEK3
HEK293T cells
Caco-2 cells
Liver org
Intestinal org
0
5
10
10
20
30
40
50
60
70
Total sequence reads (%)
6-bp deletion in CTNNB1 (S1E1)
HEK293T cells
Caco-2 cells
Liver org
Intestinal org
0
5
10
10
20
30
40
50
60
Total sequence reads (%)
correct edit
byproducts pegRNA
byproducts nickRNA

Figure 1

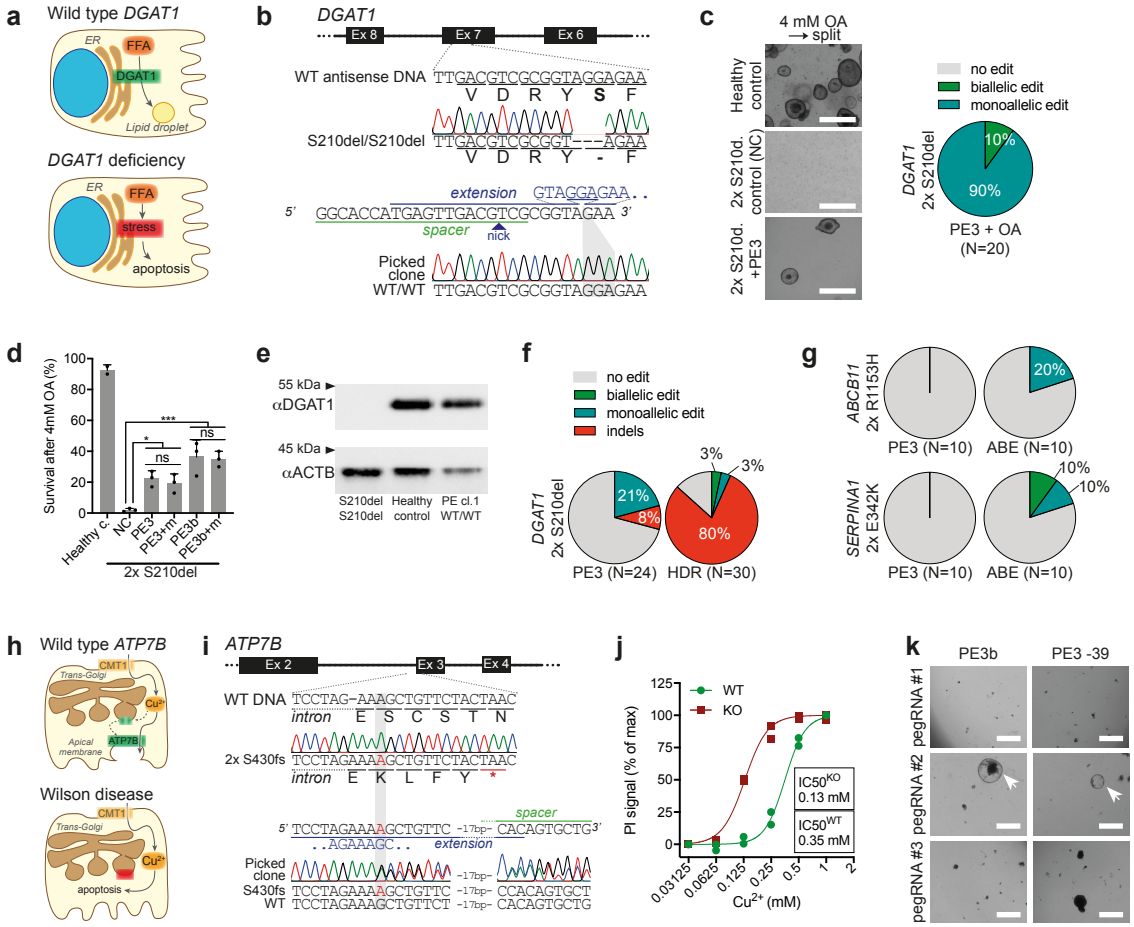
a
Wild type DGAT1
ER
FFA
DGAT1
Lipid droplet
DGAT1 deficiency
ER
FFA
stress
apoptosis
b
DGAT1
Ex 8
Ex 7
Ex 6
WT antisense DNA TTGACGTCGCGGTAGGAGAA
V D R Y S F
S210del/S210del TTGACGTCGCGGT---AGAA
V D R Y - F
extension GTAGGAGAA..
5' GGCACCATGAGTTGACGTCGCGGTAGAA 3'
spacer
nick
Picked clone
WT/WT TTGACGTCGCGGTAGGAGAA
c
4 mM OA
→ split
Healthy control
2x S210d. control (NC)
2x S210d. +PE3
no edit
biallelic edit
monoallelic edit
DGAT1 2x S210del
10%
90%
PE3 + OA
(N=20)
d
Survival after 4mM OA (%)
100
80
60
40
20
0
***
*
ns
ns
Healthy c.
NC
PE3
PE3+nr
PE3b
PE3b+nr
2x S210del
e
55 kDa
αDGAT1
45 kDa
αACTB
S210del S210del
Healthy control
PE cl.1 WT/WT
f
no edit
biallelic edit
monoallelic edit
indels
DGAT1 2x S210del
21%
8%
3%
3%
80%
PE3 (N=24)
HDR (N=30)
g
ABCB11 2x R153H
20%
PE3 (N=10)
ABE (N=10)
SERPINA1 2x E342K
10%
10%
PE3 (N=10)
ABE (N=10)
h
Wild type ATP7B
CMT1
Trans-Golgi
Cu2+
Apical membrane
ATP7B
Wilson disease
CMT1
Trans-Golgi
Cu2+
apoptosis
i
ATP7B
Ex 2
Ex 3
Ex 4
WT DNA TCCTAG-AAAGCTGTTCTACTAAC
intron E S C S T N
2x S430fs TCCTAGAAAAGCTGTTCTACTAAC
intron E K L F Y *
spacer
5' TCCTAGAAAAGCTGTTC -17bp- CACAGTGCTG 3'
..AGAAAGC.. extension
Picked clone
S430fs TCCTAGAAAAGCTGTTC -17bp- CCACAGTGCT
WT TCCTAGAAAGCTGTTCT -17bp- CACAGTGCTG
j
PI signal (% of max)
125
100
75
50
25
0
WT
KO
IC50KO 0.13 mM
IC50WT 0.35 mM
0.03125
0.0625
0.125
0.25
0.5
1
2
Cu2+ (mM)
k
PE3b
PE3 -39
pegRNA #1
pegRNA #2
pegRNA #3

Figure 2

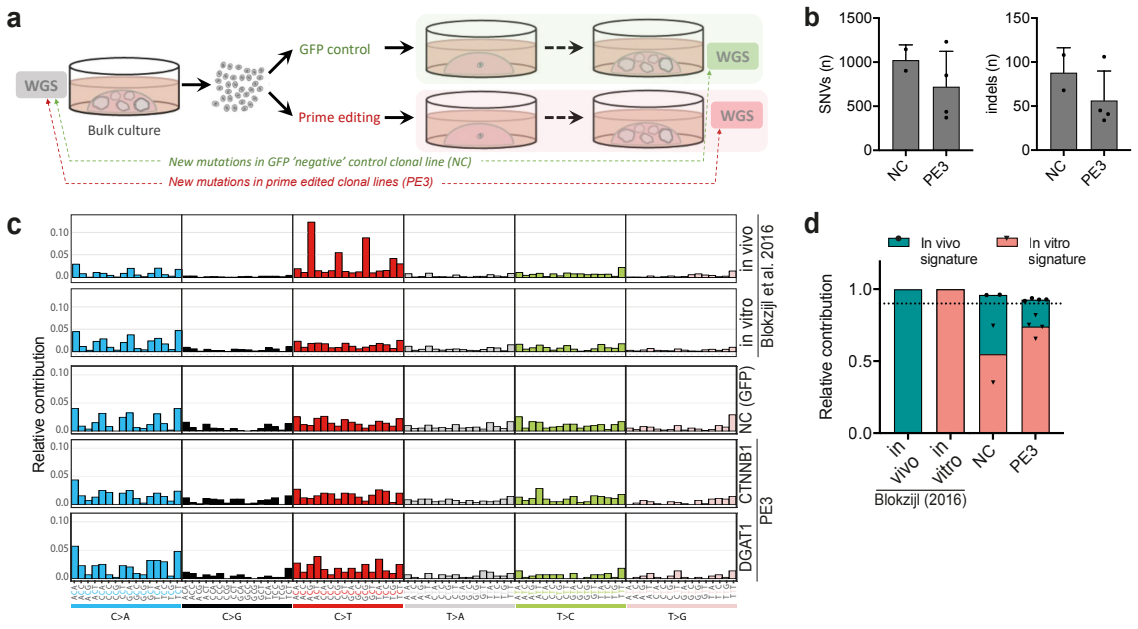
a
WGS
Bulk culture
GFP control
Prime editing
WGS
WGS
New mutations in GFP 'negative' control clonal line (NC)
New mutations in prime edited clonal lines (PE3)
b
SNVs (n)
1500
1000
500
0
NC
PE3
indels (n)
150
100
50
0
NC
PE3
c
Relative contribution
0.10
0.05
0.0
in vivo
in vitro
Blokzijl et al. 2016
NC (GFP)
CTNNB1
DGAT1
PE3
C>A
C>G
C>T
T>A
T>C
T>G
d
In vivo signature
In vitro signature
Relative contribution
1.0
0.5
0.0
in vivo
in vitro
NC
PE3
Blokzijl (2016)

Figure 3

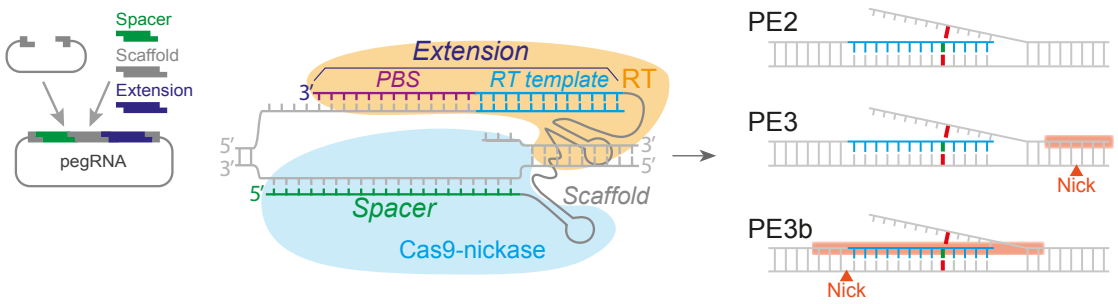

Supplementary Figure 1
Overview of the prime editing principle
Schematic representation of the pegRNA structure and the mechanism by which a pegRNA molecule binds to genomic DNA to instruct PE2 (Cas9-reverse transcriptase fusion complex) to bind to a nick a specific sequence, and synthesize a new, edited flap according to the RT template. The PE3 strategy adds a nick in the non-edited strand to enhance incorporation of the edited flap. The PE3b strategy is similar to PE3, but only nicks the opposite strand after succesful creation of an edited flap. PBS: primer binding site, RT: reverse transcriptase.

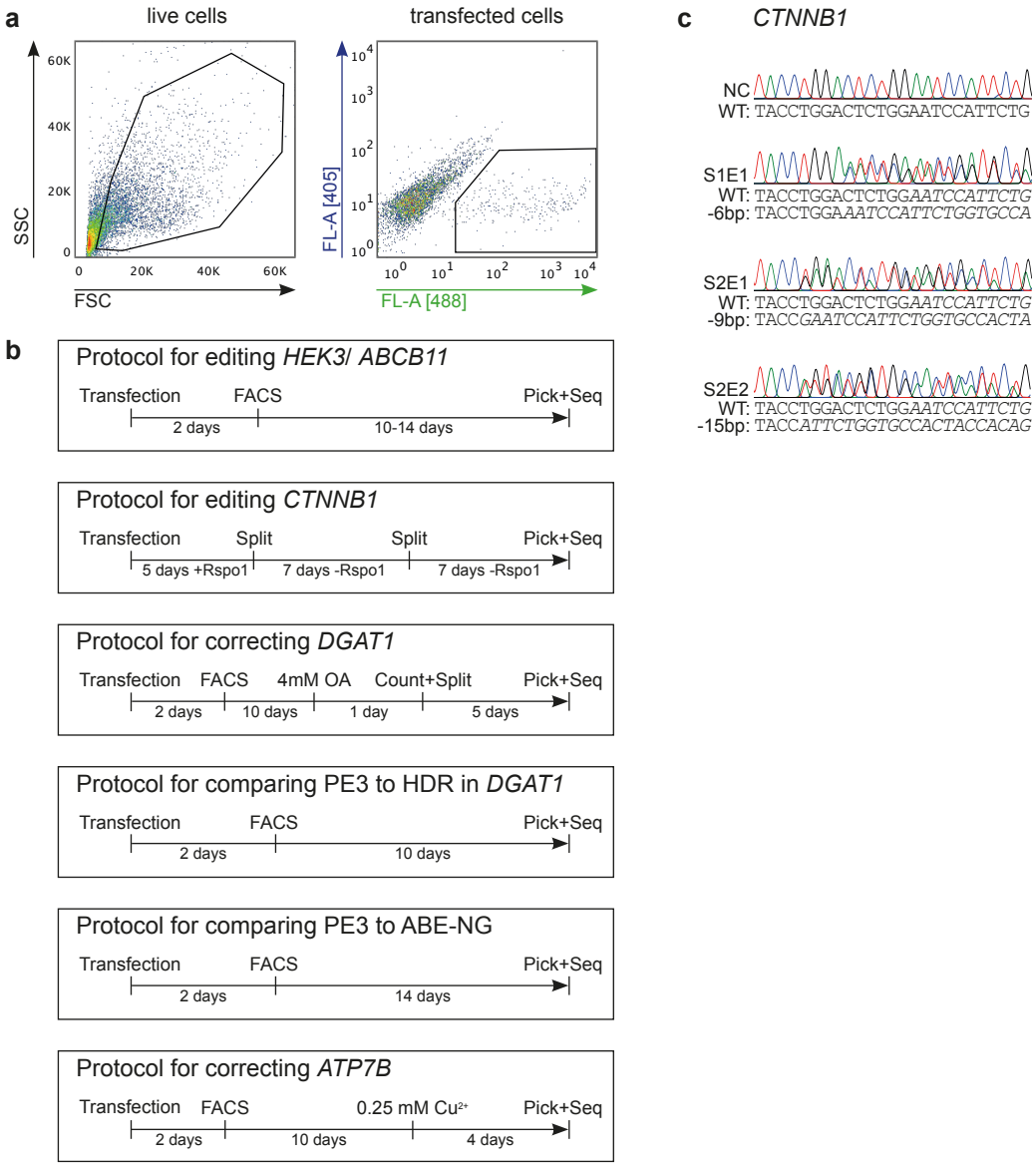

Supplementary Figure 2
Representative FACS plot example and different protocols used in this study
a, Representative FACS plot and gating strategy to sort transfected cells. Sorting of transfected cells was based on co-transfection with a GFP-reporter plasmid in all transfection experiments. **b**, Workflow and timeline for transfection of organoid cells, selection of single transfected cells, and characterization of prime editing efficiency in clonally expanded cells. Note that the workflow used for prime editing of *CTNNB1* does not contain FACS-based selection of transfected cells, but instead selects for *CTNNB1* mutants based on withdrawal of R-spondin 1 (Rspo1). **c**, Sanger validation of precise 6-bp, 9-bp, and 15-bp deletions in picked clones from *CTNNB1* pegRNA S1E1, S2E1, and S2E2, respectively. SSC: side scatter, FSC: forward scatter, OA: oleic acid.

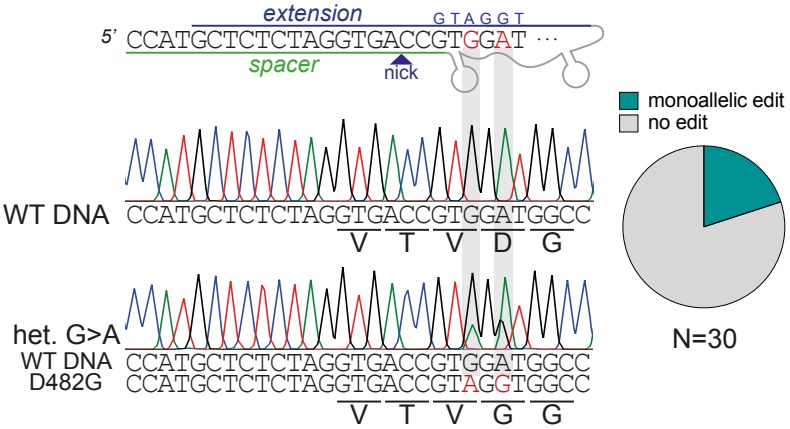

Supplementary Figure 3
Generation of *ABCB11*^{D482G} by prime editing (PE3)
Design of pegRNA and Sanger validation of generation of the pathogenic *ABCB11*^{D482G} mutation in liver organoids. Note that *ABCB11*^{D482G} is created by an A→G substitution at position 7, but the pegRNA additionally introduces a silent A→G mutation at position 5, disturbing the PAM sequence to increase efficiency.

HEK3 unwanted byproduct analysis

Pattern	%	Reads	Cell type
WT	Fig 1h	-	-
5bp del	Fig 1h	-	-
G>A +9	2.392	1198	intestinal
G>A +9	1.022	95	liver
G>A +9	0.898	114	intestinal
G>A +9	0.864	216	intestinal
G>A +9	0.685	217	HEK293T
G>A +9	0.682	295	HEK293T
G>A +9	0.534	311	HEK293T
G>A +9	0.271	73	liver
C>A +23	1.549	491	HEK293T
C>A +23	0.78	200	Caco-2
C>A +23	0.737	98	liver
C>A +23	0.528	132	intestinal
C>A +31	1.495	474	HEK293T
C>A +31	0.925	123	liver
C>A +31	0.74	185	intestinal
C>A +31	0.709	182	Caco-2
C>A +31	0.25	108	HEK293T
C>A -9	0.776	246	HEK293T
C>A -9	0.489	65	liver
C>A -9	0.444	114	Caco-2
C>A -9	0.412	103	intestinal
G>A +9	0.669	89	liver
G>A +9	0.446	193	HEK293T
G>A +9	0.444	111	intestinal
G>A +9	0.42	39	liver
G>A +9	0.302	176	HEK293T
G>A +9	0.28	140	intestinal
C>A +23	0.656	208	HEK293T
C>A +23	0.632	84	liver
C>A +23	0.394	101	Caco-2
C>A +23	0.328	82	intestinal
G>T +12	0.609	193	HEK293T
G>T +12	0.448	115	Caco-2
G>T +12	0.391	52	liver
G>T +12	0.364	91	intestinal
C>A +30	0.606	192	HEK293T
C>A +30	0.399	53	liver
C>A +30	0.277	71	Caco-2

CTNNB1 unwanted byproduct analysis

Pattern	%	Reads	Cell type
WT	Fig 1h	-	-
6bp del	Fig 1h	-	-
G>A +6	1.894	2830	intestinal
G>A +6	1.036	732	HEK293T
G>A +6	0.947	387	HEK293T
G>A +6	0.76	509	liver
G>A +6	0.759	351	HEK293T
G>A +6	0.757	1007	intestinal
G>A +6	0.588	497	intestinal
G>A +6	0.486	409	liver
G>A +6	0.454	322	Caco-2
G>A +6	0.379	172	Caco-2
G>A +6	0.358	387	Caco-2
G>A +6	0.349	241	liver
insA +7	0.976	675	liver
insA +7	0.905	762	liver
insA +7	0.859	575	liver
insA +7	0.856	1139	intestinal
insA +7	0.699	323	HEK293T
insA +7	0.602	246	HEK293T
insA +7	0.487	344	HEK293T
insA +7	0.438	199	Caco-2
insA +7	0.329	233	Caco-2
insA +7	0.299	324	Caco-2
C>A +30	0.787	558	Caco-2
C>A +30	0.768	355	HEK293T
C>A +30	0.739	622	liver
C>A +30	0.595	503	intestinal
7bp del	0.21	97	HEK293T
7bp del	0.139	57	HEK293T
7bp del	0.12	85	HEK293T
7bp del	0.09	64	Caco-2
7bp del	0.039	33	liver

Nicking location of pegRNA **bold** Substitution Insertion - Deletion

Supplementary Figure 4

Analysis of editing byproducts after prime editing in HEK293T cells, Caco-2 cells, and liver and intestinal organoid cells

Allele frequency tables of the *HEK3* and *CTNNB1* locus after prime editing (PE3) to generate a 5-bp and 6-bp deletion, respectively, directly upstream from the pegRNA nicking position. For each cell type, transfection and high-throughput amplicon sequencing was performed in three replicates. Unwanted byproducts that occured at a frequency of >0.2% were grouped by pattern to vizualize occurence in each cell type. Note that common unwanted byproduct patterns occur in all cell types, but generally at a very low rate (<1%).

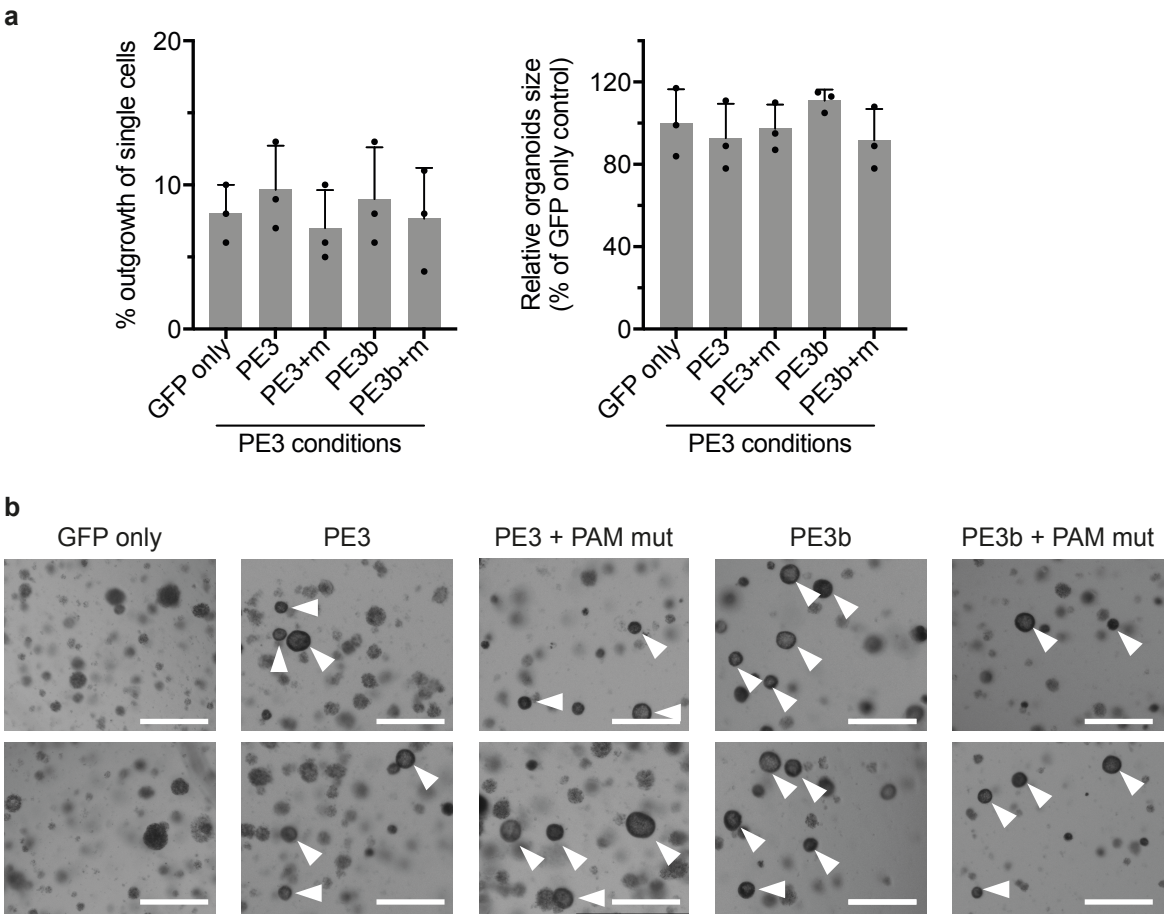

Supplementary Figure 5
Functional correction of *DGAT1*^{S210del} by prime editing (PE3)
a, Left panel represents outgrowth of single, FACS sorted patient-derived intestinal organoid cells after transfection with GFP-reporter plasmid only or with GFP-reporter plasmid and PE3 plasmids. Right panel represents relative organoid size at day 7 after seeding, which was used as a proxy to quantify proliferation capacity of organoid cells in each condition. Data are represented as mean values +/- S.D. of three independent experiments. **b,** Representative brightfield images of *DGAT1*^{S210del} patient organoids after exposure to 4 mM oleic acid for 24 hours, without (GFP only) and with prime editing (PE3/PE3b). PAM mut stands for conditions in which the PAM-site was mutated by prime editing. White arrowheads indicate surviving organoids. White scale bars are 500 µm. PE3+m: PE3 with introduction of PAM mutation. Source data are provided as a Source Data file.

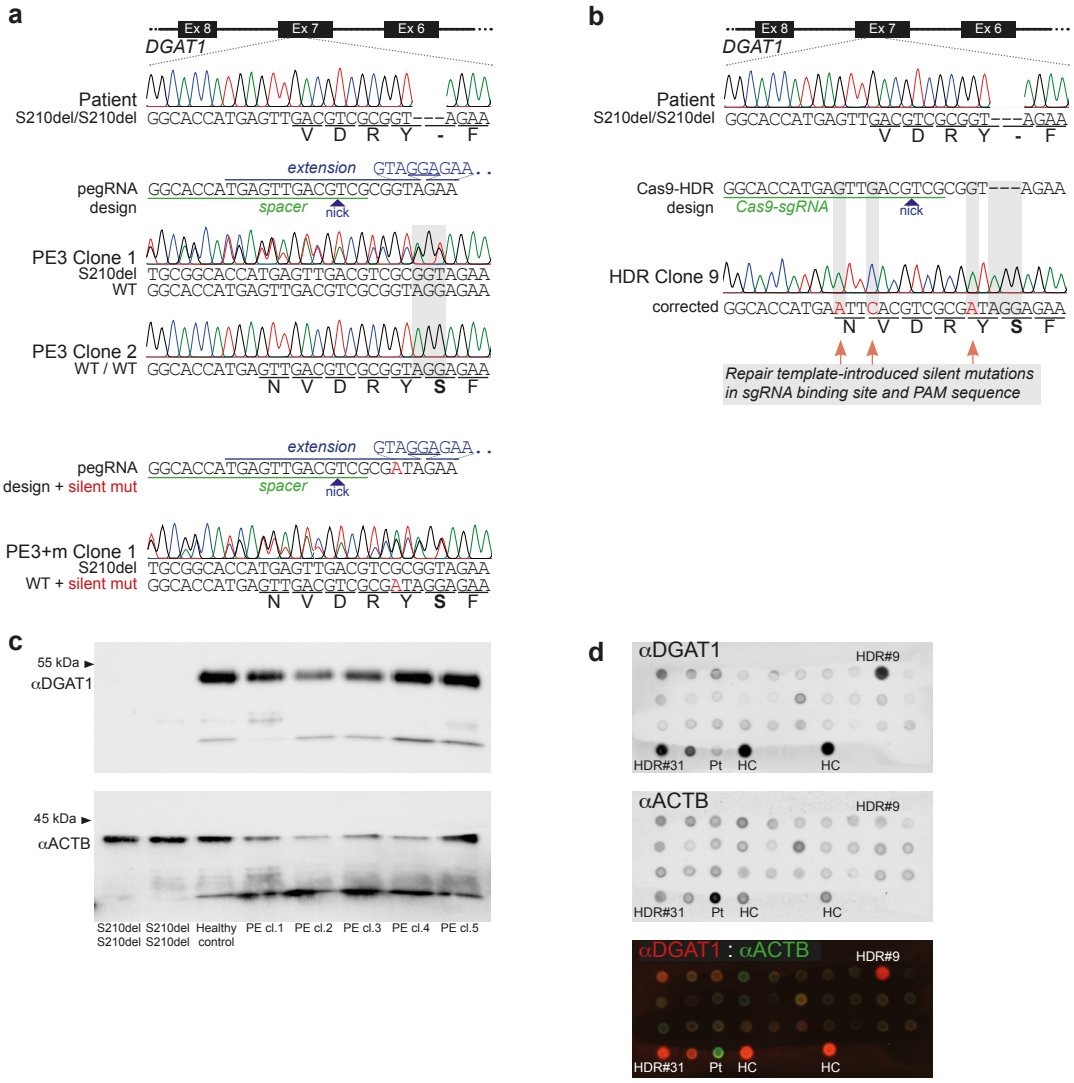

Supplementary Figure 6

Prime editing (PE3) and Cas9-mediated HDR to correct *DGAT1*^{S210del}

a, Design of the pegRNAs used in PE3 to repair the *DGAT1*^{S210del} mutation in patient-derived intestinal organoids. Sanger validation of the mutation before editing and after editing in two clonally expanded organoid lines with monoallelic and biallelic repair. Note that PE3+mutation of the PAM results in a silent mutation. **b**, Design of the sgRNA used to repair *DGAT1*^{S210del} mutation through Cas9-initiated HDR. A homology template of ±200 nucleotides flanking the DSB was used, which contained silent mutations to enhance editing. Sanger validation of the single clone with biallelic repair. **c**, Western blot validation of 5 prime edited (PE) clones. **d**, Dot blot validation of HDR corrected clones; Pt: *DGAT1*^{S210del} patient organoids; HC: healthy control organoids; HDR#9: *DGAT1*^{S210del} patient organoids after HDR correction, clone #9. Ex: exon, HDR: homology directed repair, Pt: patient, HC: healthy control.

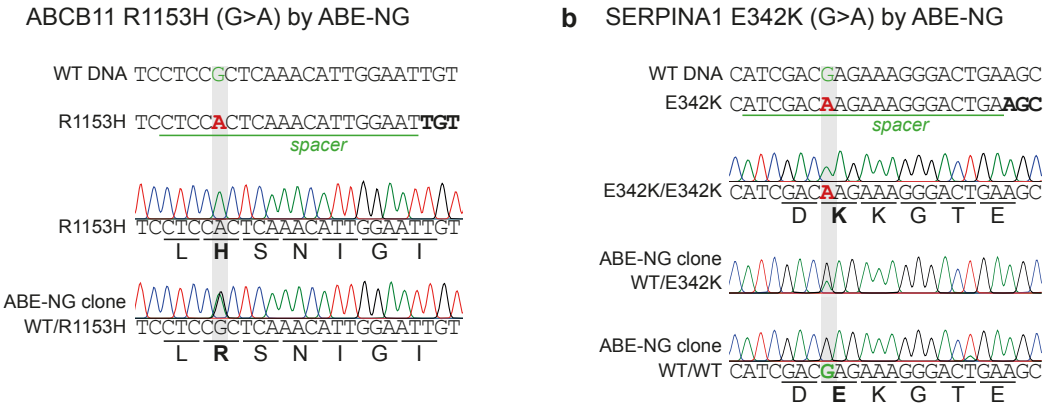

Supplementary Figure 7
Correction of *ABCB11*^{R1153H} and *SERPINA1*^{E342K} by base editing
a, Design of the sgRNA used for adenine base editing (ABE) of the *ABCB11*^{R1153H} mutation using ABEmax-NG in liver organoids derived from a patient with BSEP-deficiency. Sanger validation of monoallelic repair by ABE-NG **b,** Design of the sgRNA used for adenine base editing of the *SERPINA1*^{E342K} mutation using ABEmax-NG in liver organoids derived from a patient with alpha-1-antitrypsin deficiency. Sanger validation of monoallelic and biallelic repair by ABE-NG. The mutations in **(a)** and **(b)** were also targeted by PE3 but without success; related to Fig. 2g.

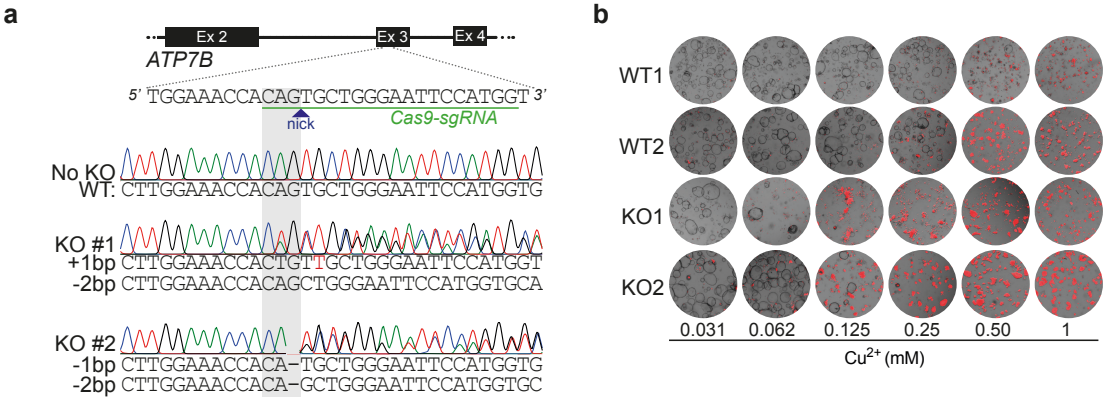

Supplementary Figure 8
Validation of a functional assay for ATP7B function
a, Design of the sgRNA used to create indels in exon 3 of *ATP7B* in liver organoids, derived from healthy controls, using a cutting Cas9. Sanger validation of two clonal *ATP7B* knock-out (KO) lines, showing heterozygous frameshift mutations. **b,** Propidium Iodide staining on wildtype and *ATP7B* knock-out liver organoids after copper exposure. Ex: exon.

a

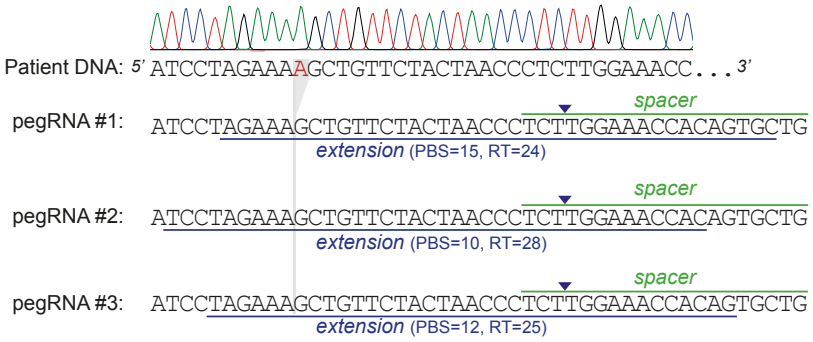

Supplementary Figure 9
PegRNA designs used for correction of *ATP7B*^{S410fs}
Schematic overview of the different pegRNAs used in an effort to correct *ATP7B*^{S410fs} mutations in liver organoids derived from a Wilson disease patient. Note that the same spacer was used, but various PBS and RT-template lenghts were tested. PBS: primer binding site, RT: reverse transcriptase template.

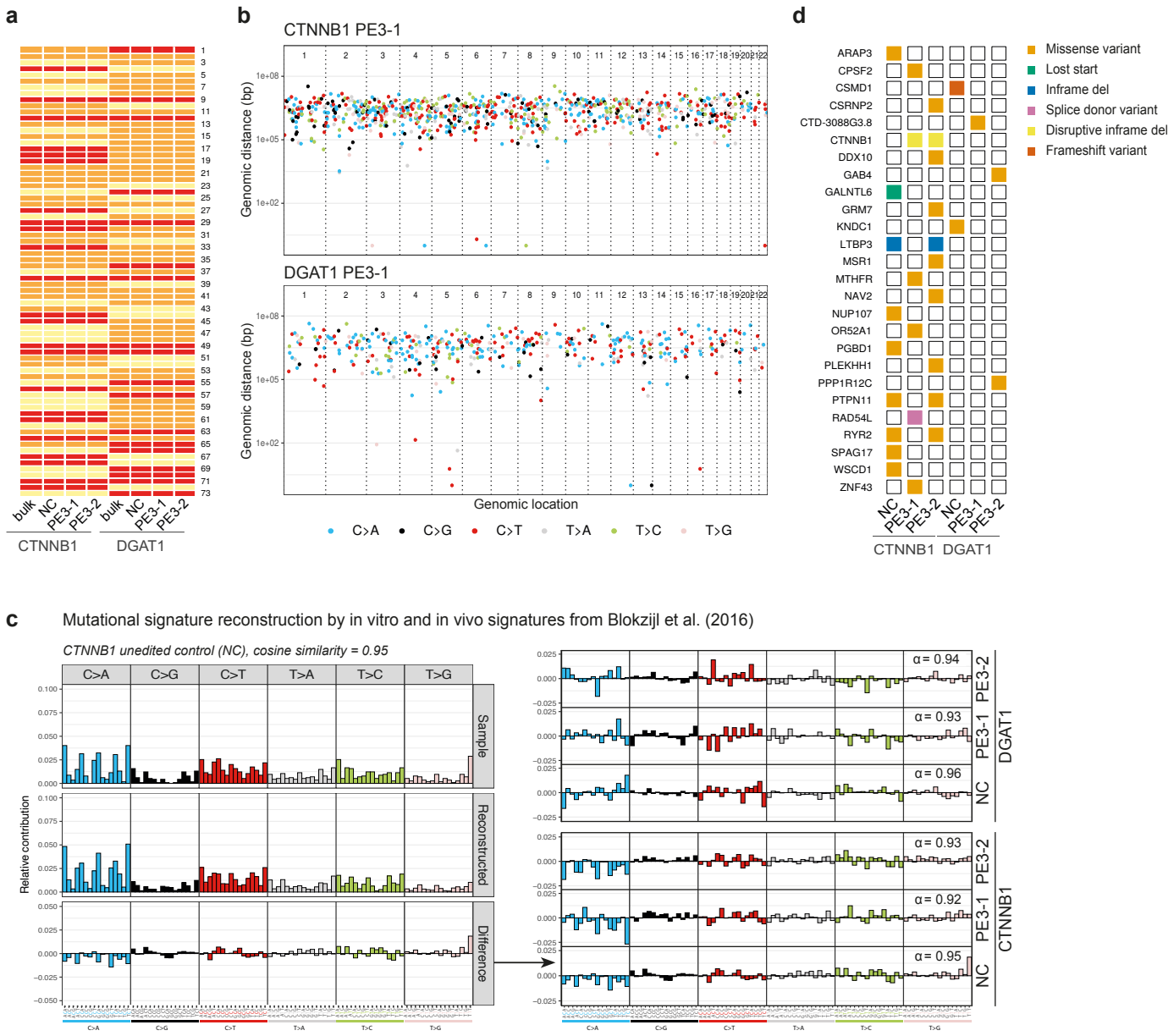

Supplementary Figure 10

Prime editing induces no genome-wide off-target effects

a, Fingerprinting of whole-genome-sequenced samples validates shared donor origin of bulk, unedited negative control (NC), and prime edited (PE3-1 and PE3-2) organoid lines. **b,** Rainfall plots of prime edited clonal organoid lines. Every new mutation, relative to the background bulk line, is indicated with a dot and is ordered by genomic location on the X axis. The Y axis shows the genomic distance between each new mutation and the one prior to it (log scale). **c,** Reconstruction of the mutational signature of prime edited and unedited control samples by *in vivo*- and *in vitro*-signatures from Blokzijl et al. (2016). Cosine similarity (α) indicates how well the reconstructed signature resembles the sample signature (1= perfect, 0.9= very well, 0= no resemblance). **d,** Overview of new variants in tumor suppressors and oncogenes from COSMIC (Forbes et al., 2017). Note that the disruptive in-frame deletions in *CTNNB1* are the intended, correct mutations of the clonal prime edited *CTNNB1* organoid lines (PE3-1 and PE3-2). Also note that prime edited samples do not acquire more mutations in the considered genes compared to negative control (NC) samples of the same donor line.

Supplementary Table 1. Sequences of pegRNAs used in prime editing experiments. All sequences are shown in 5' to 3' orientation. pegRNAs are a concatenation of the spacer sequence, the sgRNA scaffold, and the 3' extension (contains PBS and RT template (RTT)).

pegRNA	spacer sequence	3' extension sequence	PBS length (nt)	RTT length (nt)	Figure
HEK3_del1-5	GGCCCAGACTGAGCACGTGA	TGGAGGAAGCAGGGCTTCCTTTCCTCTGCCGTGCTCAGTCTG	13	29	1b,h, S4
HEK3_26CtoG	GGCCCAGACTGAGCACGTGA	TGGAGGAACCAGGGCTTCCTTTCCTCTGCCATCACGTGCTCAGTCTG	13	34	1c
CTNNB1_S1E1_del1-6	CAACAGTCTTACCTGGACTC	TGGCACCAGAATGGATTTCCAGGTAAGAC	12	17	1d,e,g,h, S4
CTNNB1_S1E2_del3-5	CAACAGTCTTACCTGGACTC	ACCAGAATGGATTCAGTCCAGGTAAGACTGT	15	16	1d,e,g
CTNNB1_S2E1_del4-12	CTGGCAGCAACAGTCTTACC	TGGTAGTGGCACCAGAATGGTAAGACTGTTGCTGCC	15	21	1d,e,g
CTNNB1_S2E2_del4-18	CTGGCAGCAACAGTCTTACC	TGGCACCAGAATGGATTCGGTAAGACTGTTGCT	12	21	1d,e,g
ABCB11-D482G-create	CCATGCTCTCTAGGTGACCG	AATGTCATGGCCACCTACGGTCACCTAGAGAGC	13	20	S3
DGAT1_ins9-11_GGA_S1E1	GGCACCATGAGTTGACGTCG	AAGCTCTTCTCCTACCGCGACGTCAACTCA	10	20	2b,c,d, S5
DGAT1_ins9-11_GGA_S1E2	GGCACCATGAGTTGACGTCG	AAGCTCTTCTCCTATCGCGACGTCAACTCA	10	20	2d, S5
ATP7B-del19-pegRNA1	CAGCACTGTGGTTTCCAAGA	AGAAAGCTGTTCTACTAATCCTCTTGGAAACCACAGTGC	15	24	2k, S9
ATP7B-del19-pegRNA2	CAGCACTGTGGTTTCCAAGA	TCCTAGAAAGCTGTTCTACTAATCCTCTTGGAAACCAC	10	28	2k, S9
ATP7B-del19-pegRNA3	CAGCACTGTGGTTTCCAAGA	TAGAAAGCTGTTCTACTAATCCTCTTGGAAACCACAG	12	25	2k, S9
ABCB11-R1153H-correct-1	AAACAATTCCAATGTTTGAG	CCAGTTCCTCCGCTCAAACATTGGAATTGT	12	18	2g, S7
ABCB11-R1153H-correct-2	CAATTCCAATGTTTGAGTGG	TGTCCAGTTCCTCCGCTCAAACATTGGAAT	12	18	2g, S7
SERPINA1-E342K-correct	TCCCCTCCAGGCCGTGCATA	TCCCTTTCTCGTCGATGGTCAGCACAGCCTTATGCACGGCCTGGAG	12	34	2g, S7

Supplementary Table 2. Sequences of nicking sgRNAs used in prime editing (PE3), HDR, Cas9-cutting, and base editing experiments. Sequence of HDR template used for HDR in *DGAT1* .

nicking sgRNA (PE3)	spacer sequence	Figure
HEK3+90	GTCAACCAGTATCCCGGTGC	1b,c,h, S4
CTNNB1+86/+93	CCACTCATACAGGACTTGGG	1d,e,g,h, S4
ABCB11_482+80	ATGGTGGTAGAGAACAGAAC	S3
DGAT1+46	GGGCTCCCTGCTGGCGCTGA	2b,c,d, S5
DGAT1_PE3b	CCTACCGCGACGTCAACTCA	2d, S5
DGAT1_PE3b+PAMmut	CCTATCGCGACGTCAACTCA	2d, S5
ATP7B_PE3b	AGCTGTTCTACTAATCCTCT	2k, S9
ATP7B-420-39	TCCATGGTGCAAACTACAGA	2k, S9
ABCB11-R1153H+45/+42	CTCTATTGGCAGATGATAGA	2g, S7
SERPINA1-E342K+54	GGGTATGGCCTCTAAAAACA	2g, S7

base edit sgRNA (ABE-NG)	spacer sequence	Figure
ABCB11-R1153H	CTCCACTCAAACATTGGAAT	2g, S7
SERPINA1-E342K	ATCGACAAGAAAGGGACTGA	2g, S7

HDR sgRNA	spacer sequence	Figure
DGAT1_HDR_sgRNA	GGCACCATGAGTTGACGTCG	2f, S6

HDR repair template	HDR template sequence
DGAT1_HDR_template	GCTGTGGAGGCCTGAGTCCACCTCTCCTGCAGTGGGCTCCCTGCTGGCGCTGATGGCGCACACCATCCTCTTCCT CAAGCTCTTCTCCTATCGCGACGTGAATTCATGGTGTCGCAGAGCCAGGGCCAAGGCTGGTGAGGGGCTGCCAGG GGCTGGGGCTGCCTGCTGGGGGGCTGGGCAGCAGCAGGGCCCCAC

Cas9-cutting sgRNA	spacer sequence	Figure
ATP7B_exon3-cas9-KO	CCATGGAATTCCCAGCACTG	S8

Supplementary Table 3. Sequences of PCR and sequencing primers used for amplification and sequencing of target regions. All sequences are shown in 5' to 3' orientation.

PCR and Seq primers	primer sequence	Figure
HEK3_PCR-Fw	ATGTGGGCTGCCTAGAAAGG	1b,c
HEK3_PCR-Rv	GGTGCTGAAAGCCACTGGGC	1b,c
HEK3_Seq-Fw	GGGAAACGCCCATGCAATTAG	1b,c
CTNNB1-ex3-PCR-Fw	AGCAGGAATCTAGTCTGGATGA	1f
CTNNB1-ex3-PCR-Rv	ACTCACTATCCACAGTTCAGCA	1f
CTNNB1-ex3-Seq-Fw	GGATGCAGTACCATTCTTCCAC	1f
ABCB11_482-PCR-Fw	CCACAATGAATTGTTCTGCAGC	S3
ABCB11-482_PCR-Rv	CCTTCTATGACCTCTTAGTTTCTCC	S3
ABCB11-482_Seq-Fw	CCACATTTCAAGAGGAATTGTTTCC	S3
DGAT1_PCR-Fw	ATGCCTGGTTATTGGTGAGC	2b, S6
DGAT1_PCR-Rv	TGAGCTCGTAGCACAAGGTG	2b, S6
DGAT1_Seq-Fw	GCATTCCAGGTTGAGAAGCG	2b, S6
ATP7B_PCR-Fw	CCCCGCATGCAGTAAGTATT	2h, S8, S9
ATP7B_PCR-Rv	AACACAATGCCAGTTATACAAGGA	2i, S7, S8
ATP7B-Seq-Fw	AGGTGAAGTTACGGGGTAGC	2i, S7, S8
ABCB11_1153-PCR-Fw	CTGTAGAGCCAGAGTTCAGG	2g, S7
ABCB11_1153-PCR-Rv	CATTCTACTTCTCCCCATCC	2g, S7
SERPINA1_342-PCR-Fw	GTCAGGAAGATGGACAGAGG	2g, S7
SERPINA1_342-PCR-Rv	GGCAGTTATTTTTGGGTGGG	2g, S7
HEK3_HTS-Fw	ACACTCTTTCCCTACACGACGCTCTTCCGATCTNNNNATGTGGGCTGCCTAGAAAGG	1h
HEK3_HTS-Rv	TGGAGTTCAGACGTGTGCTCTTCCGATCTCCCAGCCAAACTTGTCAACC	1h
CTNNB1_HTS-Fw	ACACTCTTTCCCTACACGACGCTCTTCCGATCTNNNNCAATCTACTAATGCTAATACTGTTTCG	1h
CTNNB1_HTS-Rv	TGGAGTTCAGACGTGTGCTCTTCCGATCTAAGGACTGAGAAAATCCCTGTTC	1h